Numerical Study of Aeroacoustics of an NACA0018 Airfoil with a Cavity at Various Angles of Attack

Garret C. Y. Lam* and Randolph C. K. Leung†
The Hong Kong Polytechnic University, Hong Kong, P. R. China

This paper reports the progress of a two dimensional numerical study of the aeroacoustics of NACA 0018 airfoil with a cavity at -4° and 4° angles of attack, with chord based Reynolds and free-stream Mach numbers at 2×10^4 and 0.2. In addition to the vortex shedding at the airfoil trailing edge, the shear layer at the cavity oscillates in different modes at these two angles of attack. Wavelet analyses indicate that little switching between different types of flow dynamics. The airfoil at these angles of attack produces more noise than the airfoil does at zero angle of attack. Although the presence of a cavity introduces additional acoustic generation due to cavity oscillation modes, the vortex shedding at the airfoil trailing edge remains the major acoustic generating process. Since these flow processes operates at different distant frequencies, the acoustic contribution of these processes can be easily discerned in the spectral analyses.

I. Nomenclature

c	=	Acoustic speed
$\overline{C_D}$, $\overline{C_L}$, $\overline{C_P}$	=	Time averaged drag, lift and pressure coefficients
$C'_{D,rms}$, $C'_{L,rms}$	=	Root mean squared fluctuations of drag, lift coefficient
D	=	Depth of cavity
E	=	Energy
f	=	Frequency
H	=	Frontal projection to the direction of free-stream flow
L	=	Chord length
M	=	Mach number
p	=	Pressure
r	=	Distance from airfoil trailing edge
Re	=	Chord based Reynolds number
St	=	Strouhal number
St_H	=	Strouhal number of the vortex shedding at airfoil trailing edge based on H
$St_{W,n,\alpha}$	=	Strouhal number of the n-th cavity oscillation mode based on W at α
T	=	Temperature
t	=	Time
u, v	=	Velocities in $x-$ and $y-$ directions
U_∞	=	Free stream flow velocity
W	=	Cavity width
α	=	Angle of attack
γ	=	Ratio of specific heat
η	=	Time parameter in wavelet analysis
θ	=	Angle measured from x-axis
μ	=	Viscosity
ρ	=	Density
Σ	=	Period for analysis
$\overline{\phi}$	=	Time averaged value of a quantity ϕ

*Research Fellow, Department of Mechanical Engineering, garret.lam.hk@connect.polyu.hk
†Associate Professor, Department of Mechanical Engineering, mmrleung@polyu.edu.hk, and Senior AIAA Member.

ϕ' = Fluctuation of a quantity $\phi \left(= \phi - \overline{\phi}\right)$
ϕ_{rms} = Root mean squared value of a quantity ϕ
ϕ_∞ = Quantity ϕ at free stream

II. Introduction

SMALL engineering systems such as micro air vehicle and small wind turbine often encounter low Reynolds flow ($Re < 10^5$) over airfoil so the associated flow phenomenon is a hot topic of research interest. In addition to the continuous effort on improving the airfoil structural integrity, researchers are also seeking innovative airfoil design to provide high aerodynamic performance yet low noise.

One of the potential candidates is an airfoil with a cavity. Lam and Leung [1] have recently demonstrated that at zero angle of attack α, such kind of airfoil, i.e. along the line of Kasper's concept [2], produces less noise than an airfoil without a cavity does by at least a few dB. Meanwhile, the airfoil still provides a much stronger lift than its ordinary counterpart does. The airfoil concept tries to trap air flow inside the cavity so as to create a local low pressure zone and thus additional lift. Subsequent studies [3–8] mainly focus on the aerodynamics of the airfoil while others [9, 10] on the control of trapped vortices inside the cavity.

There are only a few works dedicated to study the aeroacoustics of airfoil with cavity. Schumacher et al [11] investigated the acoustic generation of a thin plate with super-elliptic nose and tapered tail at a larger $Re \sim O\left(10^5\right)$. Up till now, the only work relevant to the aeroacoustics problem is Lam and Leung's work [1], in which via an extensive wavelet, FFT, and coherence analyses, they identified three types of acoustic generation for an airfoil at $\alpha = 0°$. They are the dominant airfoil trailing edge tone, the cavity tones, and a feedback mechanism between the cavity and the airfoil trailing edges. This work serves a continuation to Ref. [1] and aims at investigating the acoustic generation of the same airfoil with a cavity at selected α, namely $-4°$ and $4°$. The present paper reports and discusses the latest understanding of the aeroacoustic problem.

III. Formulation of the Problem

A. Direct Aeroacoustic Simulation

In the present study, we apply direct aeroacoustic simulation approach [12, 13] for its inherent capability of resolving the interaction between the flow dynamics and acoustics which is essential in studying the aeroacoustic phenomenon involving possible feedback mechanism. In this approach, the governing equations of the two dimensional flow past an airfoil, namely compressible Navier-Stokes (N-S) equations and the equation of state, are solved simultaneously. Taking the free stream parameters (denoted by subscript ∞) as reference scales, the N-S equations in dimensionless strong conservative form can be written as

$$\frac{\partial \boldsymbol{U}}{\partial t} + \frac{\partial \left(\boldsymbol{F} - \boldsymbol{F_v}\right)}{\partial x} + \frac{\partial \left(\boldsymbol{G} - \boldsymbol{G_v}\right)}{\partial y} = 0, \tag{1}$$

where $\boldsymbol{U} = [\rho, \rho u, \rho v, \rho E]^{\mathrm{T}}$, $\boldsymbol{F} = \left[\rho u, \rho u^2 + p, \rho uv, (\rho E + p)\, u\right]^{\mathrm{T}}$, $\boldsymbol{G} = \left[\rho v, \rho uv, \rho v^2 + p, (\rho E + p)\, v\right]^{\mathrm{T}}$, $\boldsymbol{F_v} = \left[0, \tau_{xx}, \tau_{xy}, \tau_{xx}u + \tau_{xy}v - q_x\right]^{\mathrm{T}} / Re_\infty$, $\boldsymbol{G_v} = \left[0, \tau_{xy}, \tau_{yy}, \tau_{xy}u + \tau_{yy}v - q_y\right]^{\mathrm{T}} / Re_\infty$ with u and v being the velocities in x and y directions respectively, $\tau_{xx} = \frac{2}{3}\mu\left(2\frac{\partial u}{\partial x} - \frac{\partial v}{\partial y}\right)$, $\tau_{xy} = \mu\left(\frac{\partial u}{\partial y} + \frac{\partial v}{\partial x}\right)$, $\tau_{yy} = \frac{2}{3}\mu\left(2\frac{\partial v}{\partial y} - \frac{\partial u}{\partial x}\right)$, $E = \frac{p}{\rho(\gamma-1)} + \frac{u^2+v^2}{2}$, $p = \frac{\rho T}{\gamma M_\infty^2}$, $q_x = -\frac{\mu}{(\gamma-1)Pr_\infty M_\infty^2}\frac{\partial T}{\partial x}$, $q_y = -\frac{\mu}{(\gamma-1)Pr_\infty M_\infty^2}\frac{\partial T}{\partial y}$, the specific heat ratio $\gamma = 1.4$, free stream Mach number $M_\infty = \widehat{U}_\infty / \sqrt{\gamma \widehat{R}\widehat{T}_\infty}$, specific gas constant $\widehat{R} = 287.058 J/(kgK)$ for air, $Re_\infty = \widehat{\rho}_\infty \widehat{U}_\infty \widehat{L} / \widehat{\mu}_\infty$ and Prandtl number $Pr_\infty = \widehat{c_{p,\infty}}\widehat{\mu}_\infty / \widehat{k}_\infty = 0.71$.

The governing equations are solved by the conservation element and solution element (CE/SE) method, which has been successfully applied in investigating aeroacoustics of compressible flows such as jet screech [14, 15] since its introduction. Lam et al. [12] further systemically established its capability of capturing interactions between flow and acoustics accurately via a series of benchmark aeroacoustic problems at low Mach number.

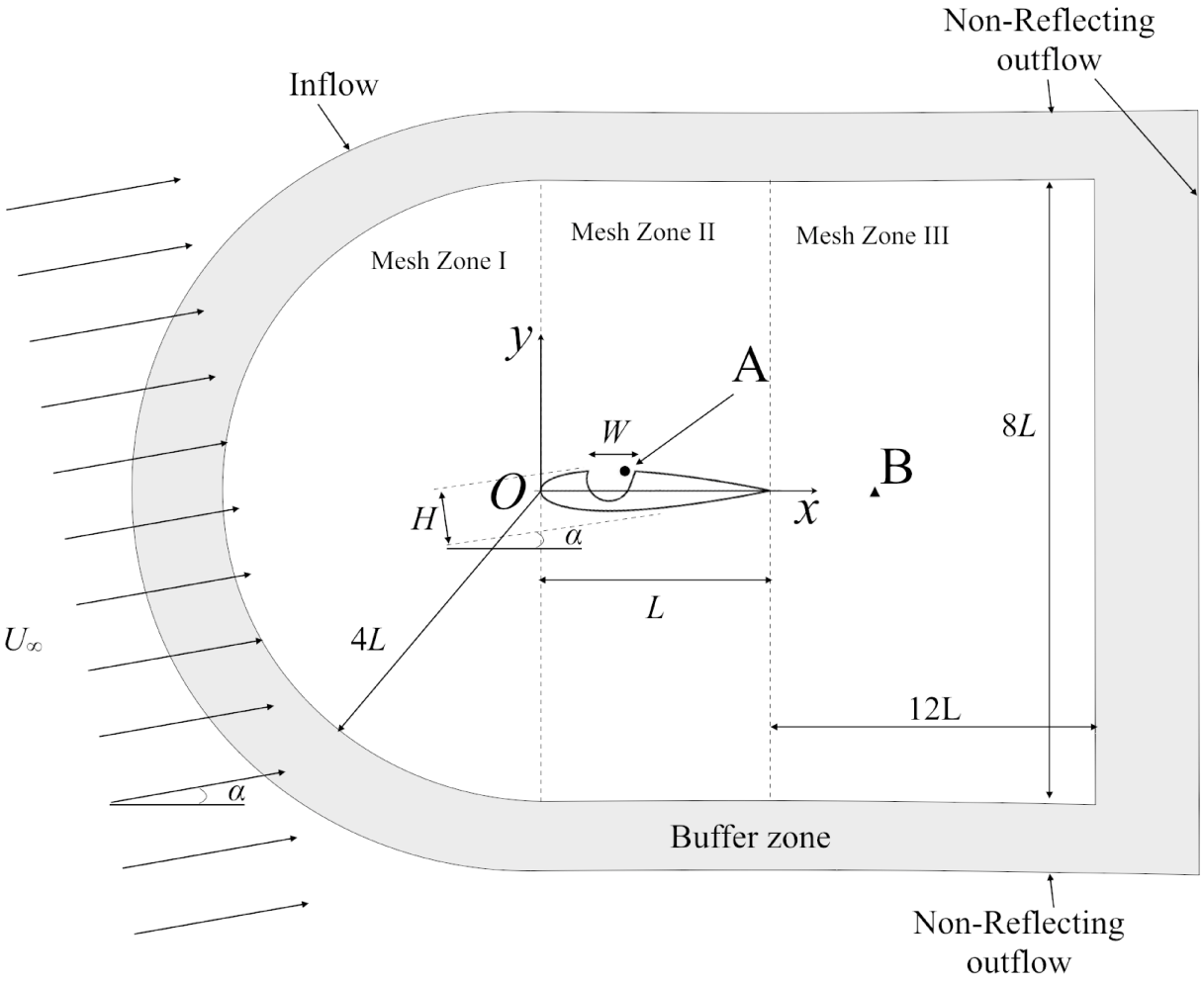

Fig. 1 Schematic sketch of the computational domain. ●, Probe A; ▲, probe B.

B. Numerical Setup

Figure 1 illustrates the computational domain. The present airfoil with cavity replicates that in Olsman's work [16]. The dimensions of cavity are $W = 0.21L$ and its depth $D = 0.16L$. The airfoil geometry follows the description given in Ref. [16]. H is the frontal projection to the direction of free stream flow and varies with different α. C-grid approach is adopted in the mesh, which is divided into 4 zones (Mesh Zone I, II, III and buffer zone). The mesh in each zone is clustered near the airfoil and is stretched toward the boundary. The mesh parameters of all zones are listed in Table 1.

Inflow with $M_\infty = 0.2$ and $Re_\infty = 2\times10^4$ sweeps through the whole domain from the inflow boundary at $\alpha = -4°$ and $4°$ and leaves the domain at non-reflecting outflow (NRBC). Near the inflow and NRBC, buffer zone with exponentially grid stretching is added to further dissipate the outgoing waves, thus minimizing their numerical reflection. No-slip boundary condition is applied to the airfoil. The computations proceed from initially stagnant state to time stationary state. Afterward, the calculations continue for a period $\Sigma = 20$ with saving intervals $t_s = 0.002$. This corresponds to $10,000$ snapshots in Σ. Probes A and B at $(x, y) = (0.388, 0.086)$ and $(1.5, 0.0)$ respectively are set for spectral analyses of vortex shedding inside the cavity and of the airfoil wake.

IV. Results and Discussions

In this section, we will firstly explore the time averaged results to investigate the aerodynamic performance of the airfoil at various α. The calculated results will be compared with those at $\alpha = 0°$ [17]. Then we will discuss the

Table 1 Mesh parameters.

Mesh	Zone I	Zone II	Zone III	Buffer zone
Minimum size	0.001	0.001	0.001	0.05
Maximum size	0.05	0.05	0.05	1.25

unsteady flow dynamics, followed by the discussion of the associated acoustic generation.

A. Time Averaged Results

Figure 2 shows the time averaged pressure coefficient $\overline{C_p} = 2\left(\overline{p} - p_\infty\right)/\rho U_\infty^2$ of $\alpha = -4°$, $0°$, and $4°$. On the airfoil upper surface of all studied α, $\overline{C_p}$ changes abruptly at the cavity on all α. Inside the cavity, $\overline{C_p}$ gradually decreases towards the cavity trailing edge where it increases suddenly. Further downstream, $\overline{C_p}$ increases smoothly except near the airfoil trailing edge, where it decreases again indicating the vortex shedding there. At $\alpha = -4°$, $\overline{C_p}$ on the airfoil upper surface is larger than that on the airfoil lower surface. This suggests a strong recirculation near the lower surface. At positive α, the situation is the opposite. However, downstream of the cavity at $\alpha = 4°$, $\overline{C_p}$ on the upper surface is larger than that on the lower surface. This may lead to a reduction of lift force in this section of airfoil.

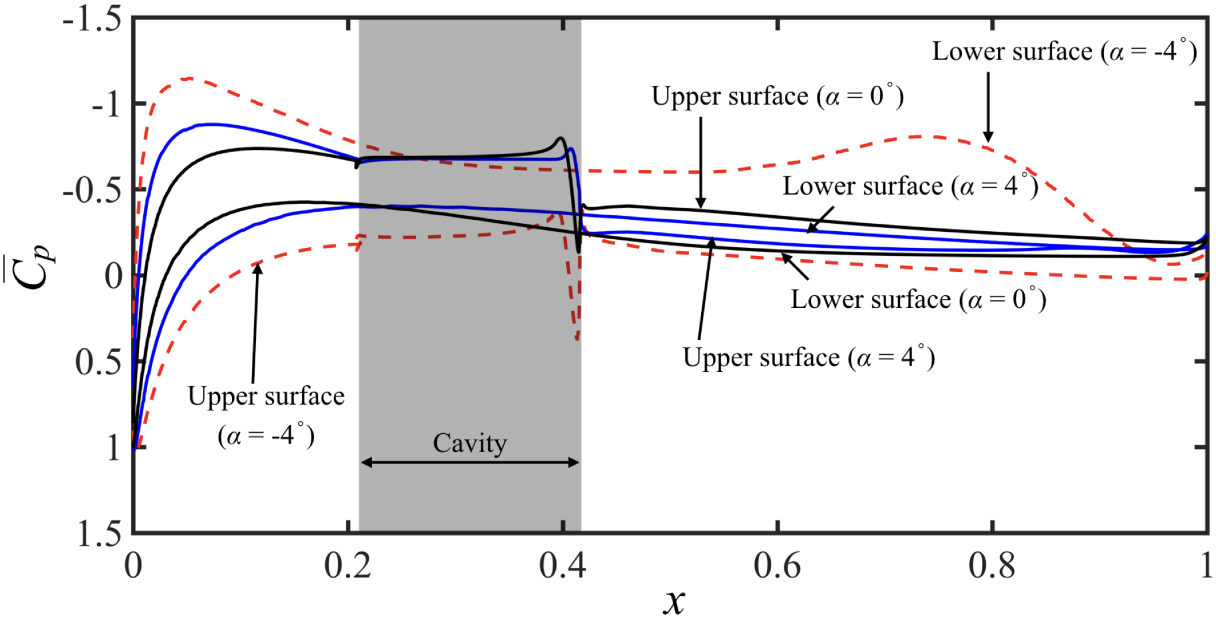

Fig. 2 Time averaged pressure coefficient $\overline{C_p}$ at $\alpha = -4°$ (Red line), $0°$ (Black line), and $4°$ (Blue line)

.

Table 2 lists the calculated time averaged lift coefficients and drag coefficients including the numerical results reported in the literature [7]. The coefficients of $\alpha = -4°$ match those in the literature closely. Though the value of $\overline{C_D}$ at $\alpha = 4°$ agrees with the results of Olsman and Colonius [7], $\overline{C_L}$ yields a much weaker lift.

Figure 3 illustrates the distribution of velocity $\overline{u}$ at $\alpha = -4°$ and $\alpha = 4°$ with streamlines. Evidently in each case, boundary layers develop on both sides of the airfoil, but the flow separates on the suction side only. Massive flow separation occurs around quarter chord at $\alpha = -4°$. At $\alpha = 4°$, the flow separation occurs near 70% chord but with a small extent. On the other hand, there are at least two recirculating zones inside the cavity for both cases. At $\alpha = -4°$ (Fig. 3c), the developed shear layer undergoes an abruptly enlargement near one third of the cavity length from the cavity leading edge and then reattaches to the cavity trailing edge. Similar observation is also found in the airfoil at $\alpha = 0°$. At $\alpha = 4°$ (Fig. 3d), the shear layer develops smoothly over the cavity after it leaves the cavity leading edge.

The rms values of velocity fluctuations u'_{rms} and v'_{rms} are shown in Fig. 4. All the recirculating zones in Fig. 3 show

Table 2 Lift coefficients and drag coefficients.

α	$\overline{C_L}$	$C'_{L,rms}$	$\overline{C_D}$	$C'_{D,rms}$
$-4°$	-0.594	0.157	0.797	0.030
$-4°$ (Olsman [7])	~ -0.538	–	~ 0.762	–
$-4°$ without cavity (Olsman [7])	~ -0.615	–	~ 0.075	–
$4°$	0.154	0.125	0.043	0.011
$4°$ (Olsman [7])	~ 0.461	–	~ 0.050	–
$4°$ without cavity (Olsman [7])	~ 0.615	–	~ 0.075	–

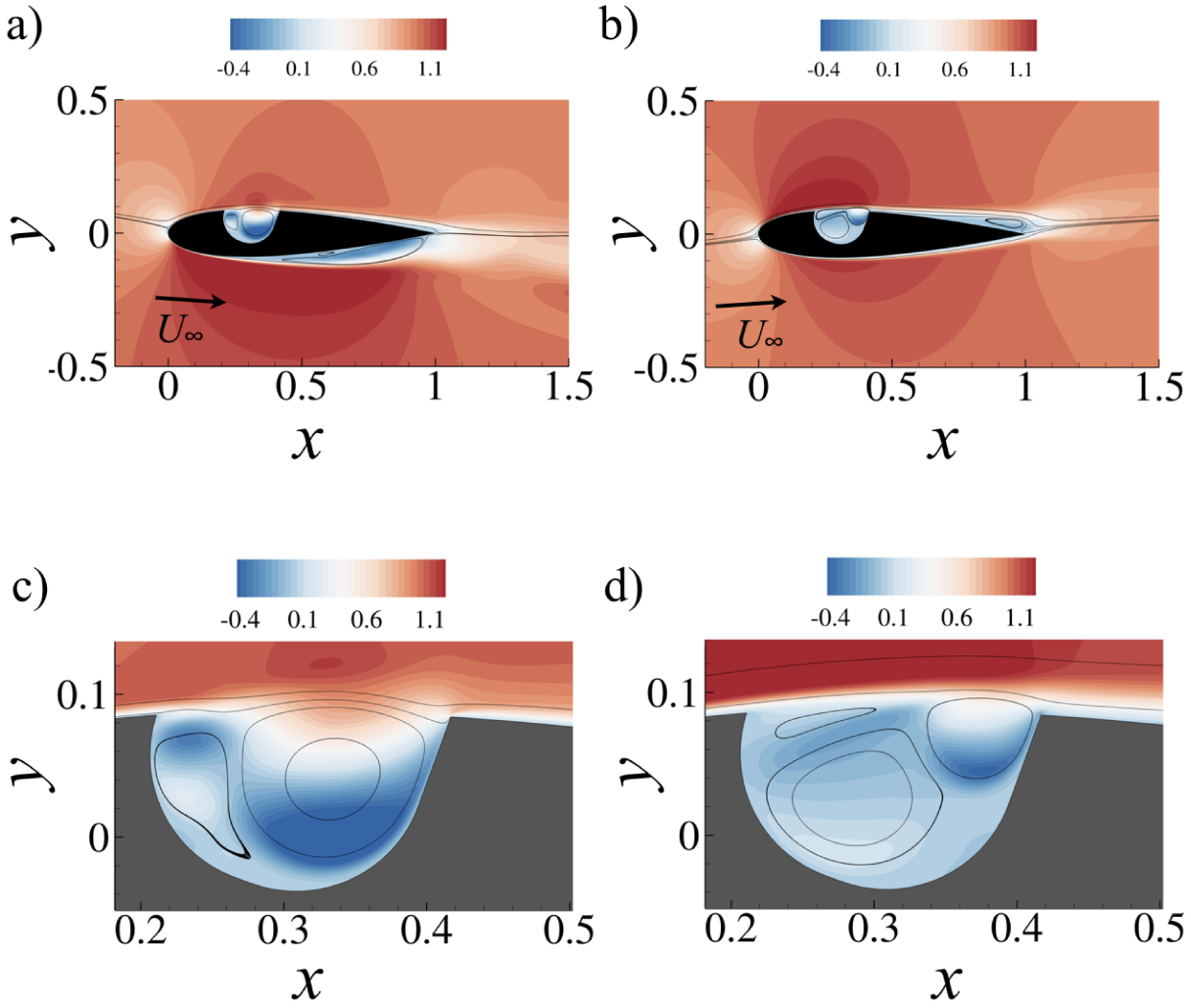

Fig. 3 Distribution of time averaged streamwise velocity $\overline{u}$ with streamlines. a) $\alpha = -4°$ with zoomed view c), b) $\alpha = 4°$ with zoomed view d).

a high level in u'_{rms} and v'_{rms}. At $\alpha = -4°$, the flow fluctuates strongly inside the whole cavity as indicated by large u'_{rms} and v'_{rms}. Furthermore, both u'_{rms} and v'_{rms} in the flow separations at the suction side are higher than those inside the cavity. This indicates that the dominant flow dynamics is vortex shedding at this flow separation as shown in the next section. The situation is similar at $\alpha = 4°$. Nevertheless, both u'_{rms} and v'_{rms} only exhibit rather weak levels in the shear layer above the cavity, rather than the whole cavity. In essence, the flow dynamics at $\alpha = 4°$ is weaker than those

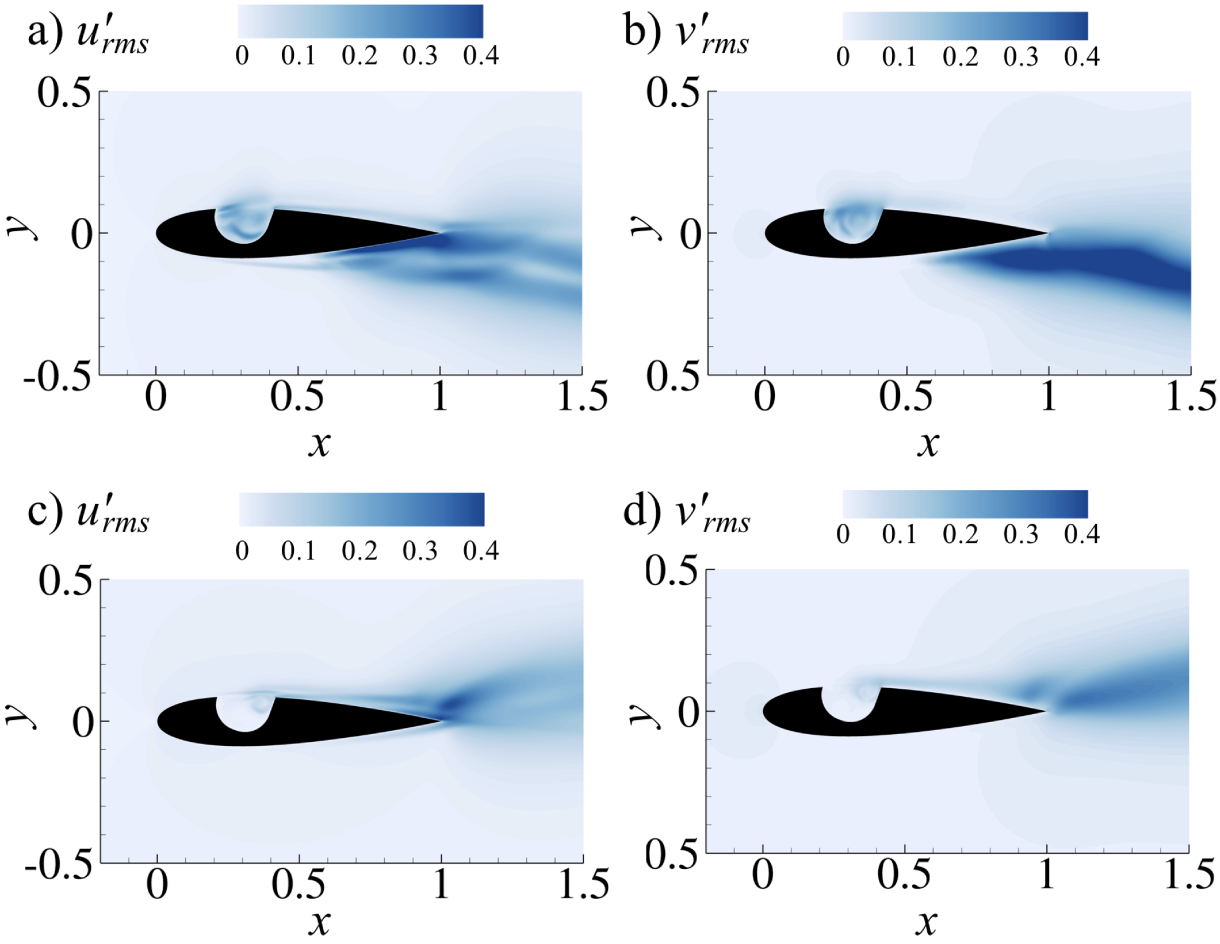

Fig. 4 Distribution of root mean squared values of velocity fluctuations u'_{rms} and v'_{rms}. a) & b) $\alpha = -4°$; c) & d) $\alpha = 4°$.

at $\alpha = -4°$.

B. Unsteady Flow Dynamics

Figure 5 illustrates the distribution of vorticity near the airfoil. At $\alpha = -4°$, the shear layer on the suction side rolls up and shed vortices at $x \sim 0.5$. The shed vortices are then convected downstream and leave the airfoil. On the pressure side, the shear layer rolls up quickly and sheds vortices after leaving the cavity leading edge. This creates a vigorous flow dynamics inside the cavity, akin to the first shear layer mode, i.e. Mode I defined in literature [1]. The second shear layer mode (Mode II in Ref. [1]) is however not observed. The finding is also consistent with that reported in Ref. [7]. At $\alpha = 4°$, the shear layer on the pressure side generally stays attached on the airfoil and rolls up to shed vortices from the airfoil trailing edge forming the vortex street in the wake. On the suction side, the shear layer over the cavity only undergoes mild oscillations and creates vortices downstream of the cavity in Mode II oscillation. A vortical structure attaches inside the cavity near the cavity trailing edge. Secondary vortices are induced at the cavity trailing edge and convected to the interior of the cavity. Nevertheless, Mode I oscillation is not observed in this case. This agrees with the observations in Olsman's work [16]. In these two cases, only one mode exists in the cavity flow unlike the case at $\alpha = 0°$, in which both Mode I and II switches alternatively. Downstream of the cavity, vortex shedding from this shear layer is also observed. The shed vortices sometimes coalesce into a large vortical structure before leaving the airfoil. These structures may draw the shear layer at the pressure side to the suction side before rolling up into vortices.

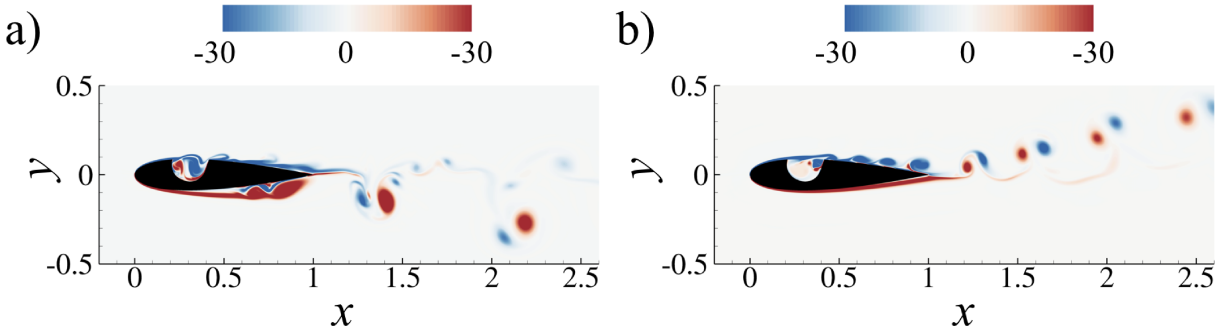

Fig. 5 Snapshots of vorticity at a) $\alpha = -4°$ **and b)** $\alpha = 4°$**.**

1. Spectral Analysis

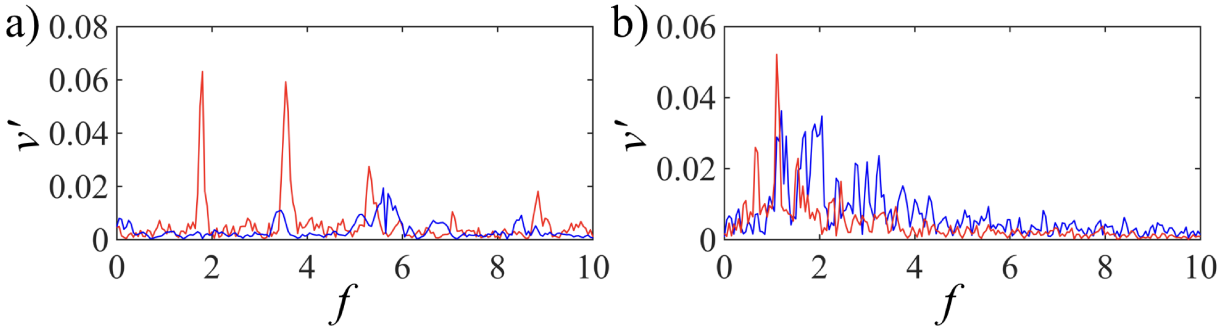

Fig. 6 Spectrum of v' **at** $\alpha = -4°$ **(red line) and** $\alpha = 4°$ **(blue line). a) Probe A; b) probe B.**

The spectra of v' at probe A and B are obtained via fast Fourier transform (FFT), in which Hamming window is applied without any data overlapping and illustrated in Fig. 6. At probe A near the cavity trailing edge, dominant peaks can be easily identified in both cases (Fig. 6a). At $\alpha = -4°$, the dominant Strouhal numbers scaled with the width of the cavity W, $St_{W,1,-4°}$, is 0.37, i.e. the frequency of Mode I oscillation. The second peak at $St_{W,2,-4°} = 0.74$ also has similar amplitudes of fluctuation. The frequency is quite close to the wake mode indicated in Ref. [7]. Other peaks are the harmonics of $St_{W,1,-4°}$. At $\alpha = 4°$, Mode II oscillation operates at $St_{W,2,4°} = 1.15$. Olsman and Colonius [7] observed that the forcing of the separation bubble by the shear layer oscillation dominates the flow dynamics inside the cavity at $St_W \sim 0.7$ in their calculations. However, in the present study, such forcing is rather weak (peak at $f = 3.45$, i.e. $St_{W,1,4°} = 0.7$) compared to Mode II oscillation.

At probe B in the wake of the airfoil, the shear layers on the suction side in both cases shed vortices at a lower frequency than the flow unsteadiness inside the cavity does. At $\alpha = -4°$, the frequency of this vortex shedding is found to be 1.1. This value corresponds to Strouhal number based on H, $St_H = 0.215$, which matches closely with that reported by Olsman and Colonius [7]. This frequency is completely different from those observed at probe A, implying a weak interaction between the flow unsteadiness at the cavity and those at the shear layer on the suction side. At $\alpha = 4°$, one should note that probe B lies marginally within the wake region of the airfoil. Multiple peaks with comparable magnitudes are present, thus it is difficult to determine the dominant vortex shedding frequency. By inspecting the vorticity distribution at various time, the vortex shedding is affected by the coalescence of the vortices downstream of the cavity. Since this coalescence acts at different frequencies, it creates multiple vortex shedding frequencies at the airfoil trailing edge.

2. Wavelet Analysis

In our previous study with $\alpha = 0°$ [1], switching of dominant flow unsteadiness near cavity was revealed and established by wavelet analysis of data captured by the probes. Therefore, we also perform wavelet analysis for the time signals v' at both probe A and B to check if any switching of flow dynamics occurs. In this analysis, the complex

Morlet wavelet function with central frequency at 6 is chosen and 20, 000 uniform intervals are used in the scales that corresponds to the interested range of frequency between 0.01 and 10. Zero padding is applied to the data so that the total lengths of the data are increased to the next higher power of 2.

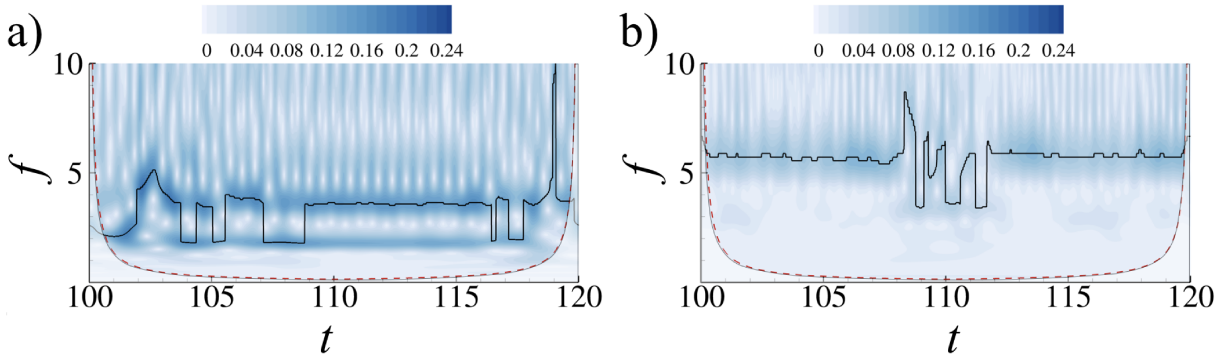

Fig. 7 Magnitude of v' wavelet spectra at Probe A. a) $\alpha = -4°$; b) $\alpha = 4°$.

Figure 7 illustrates the magnitude of v' wavelet spectra at Probe A. The red dashed lines denote the boundaries of cone of influence below which the results are ignored due to the excessive influence of zero padding. The black solid lines depict the loci of the maximum amplitude. In essence, unlike the case of $\alpha = 0°$ [1], flow dynamics near the cavity at both α is rather stable with little switching between different types. At $\alpha = -4°$, the flow dynamics stays at $St_{W,2,-4°} = 0.74$ most of the time (Fig. 7a), rather than $St_{W,1,-4°} = 0.37$ as observed in the FFT spectrum in Fig. 6a. However, both types are observed in the wavelet spectrum. The dominant flow dynamics of probe A observed in the wavelet spectrum agrees with that reported in Ref. [7]. In Fig. 7b, the flow dynamics near the cavity at $\alpha = 4°$ is dominated by Mode II oscillation except in the period $108 < t < 112$. By inspecting the evolution of vorticity in this period, the vortical structure attached to the cavity trailing edge in Fig. 5b rotate at decreasing speeds.

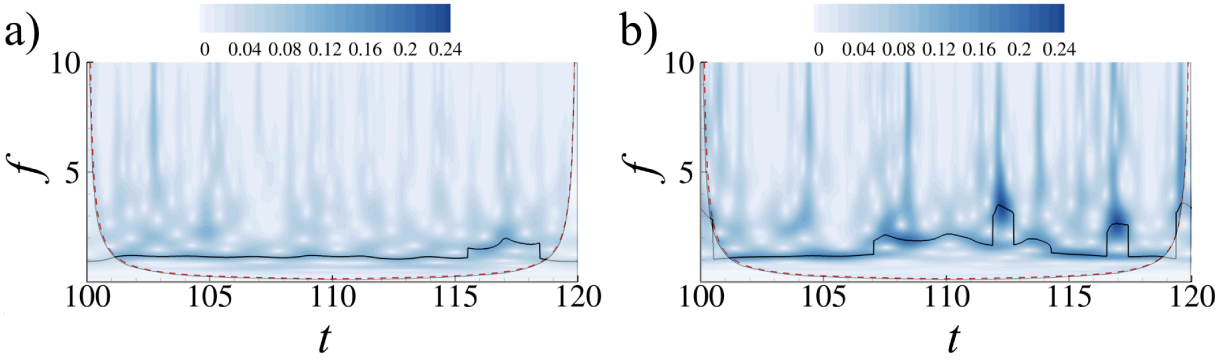

Fig. 8 Magnitude of v' wavelet spectra at Probe B. a) $\alpha = -4°$; b) $\alpha = 4°$.

At Probe B, the wavelet spectra also show quite stable phenomena (Fig. 8). The dominant flow dynamics does not change too much in the analyzing period. At $\alpha = -4°$, the maximum amplitude remains at $St_H = 0.215$ in nearly the whole period (Fig. 8a). This confirms the weak interaction between the flow dynamics near the cavity and that at the shear layer on the suction side as indicated in the FFT spectra. Their interaction is also not very large at $\alpha = 4°$ (Fig. 8b). Although the locus of maximum magnitude switches between different frequencies, these frequencies differ from those of active flow dynamics near the cavity (Probe A). The changes are caused by the coalescence of the vortices shed from the cavity before they are convected to the airfoil trailing edge.

C. Acoustic Generation

The acoustic fluctuation p' at $r = 3.5$ centering at the airfoil trailing edge are further analyzed to determine the acoustic generation. In general, p' within $\pm 20°$ measured from x-axis will be ignored because the strong flow dynamics

there conceal the propagation of acoustic wave.

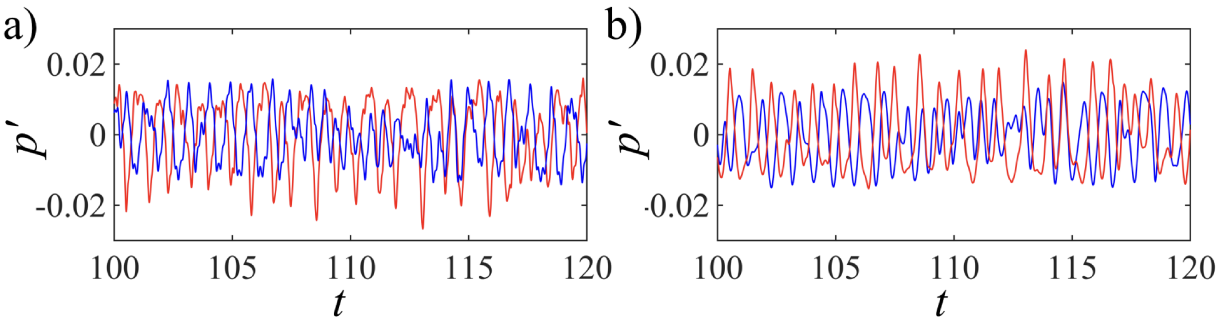

Fig. 9 Time traces of acoustic fluctuation p' at $\alpha = -4°$ (red line) and $\alpha = 4°$ (blue line). a) $(1.0, 3.5)$**; b)** $(1.0, -3.5)$**.**

Figure 9 shows the time traces of p' at $(1.0, 3.5)$ and $(1.0, -3.5)$ in both cases. The magnitudes of p' at both locations are comparable. Furthermore, p' at both α show periodicity with several dominant frequencies. Besides, p' in the upper side of the airfoil exhibit more irregularity than that in the lower side does due to the fact that the presence of cavity in the upper side creates additional flow dynamics. Fig. 10 displays the instantaneous p' at both α. The acoustics in both cases seem to be originate from the cavity and airfoil trailing edge. They also exhibit upstream preferences and asymmetric distribution owing to the nonzero α. Furthermore, the acoustic generation is dominated by the flow dynamics at the airfoil trailing edge at both α.

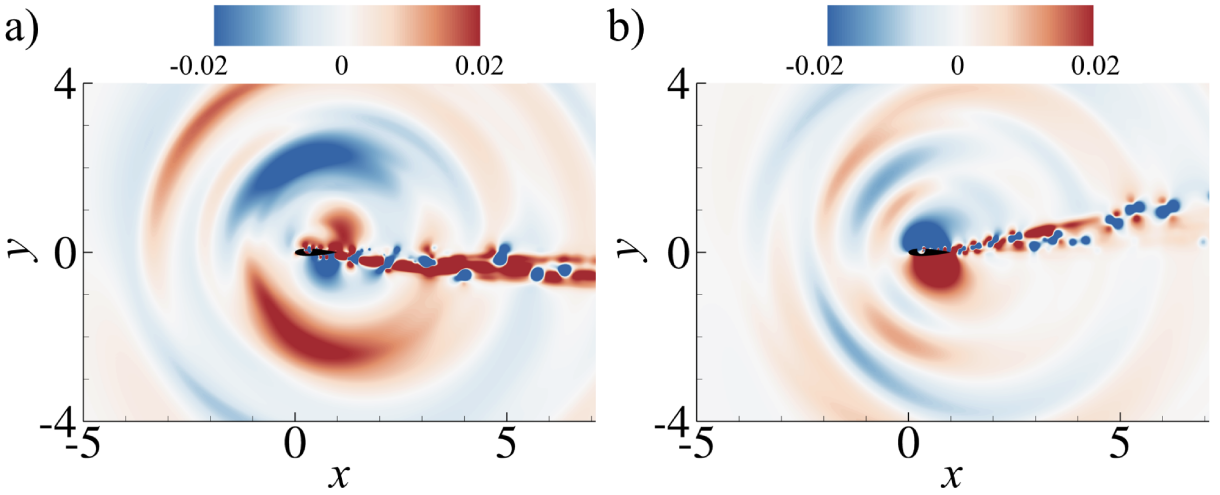

Fig. 10 Snapshots of p' at a) $\alpha = -4°$ and b) $\alpha = 4°$.

In order to get a clearer picture of the acoustic directivity, we estimated the directivity of acoustic power with the following procedures. First, the line at $r = 3.5$ was divided into 360 uniform sections. The instantaneous acoustic intensity I_{ac} at the ends of each section was calculated via the definition provided by Morfey [18]. The intensities were then integrated along each section to obtain the instantaneous acoustic power normal to each section. Finally, we integrated the instantaneous acoustic power of each section over Σ to yield the total acoustic power passing through each section. Fig. 11 shows the results at $\alpha = -4°$ and $\alpha = 4°$. The acoustic power at $\alpha = 0°$ is also shown in the figure for comparison. Firstly, the acoustic powers at both nonzero α are greater than that at $\alpha = 0°$. The acoustics at $\alpha = -4°$ is the noisiest among the three α studied. Secondly, the acoustic generation in both cases are roughly symmetric about the chord. In contrast, that at $\alpha = 0°$ shows a preference in the upper side of the airfoil, where the cavity is mounted. This implies that the flow dynamics at the airfoil trailing edge dominates the acoustic generation at these α. Otherwise, the acoustic generation due to the cavity shows up in the directivity in the second quadrant similar to that observed at $\alpha = 0°$.

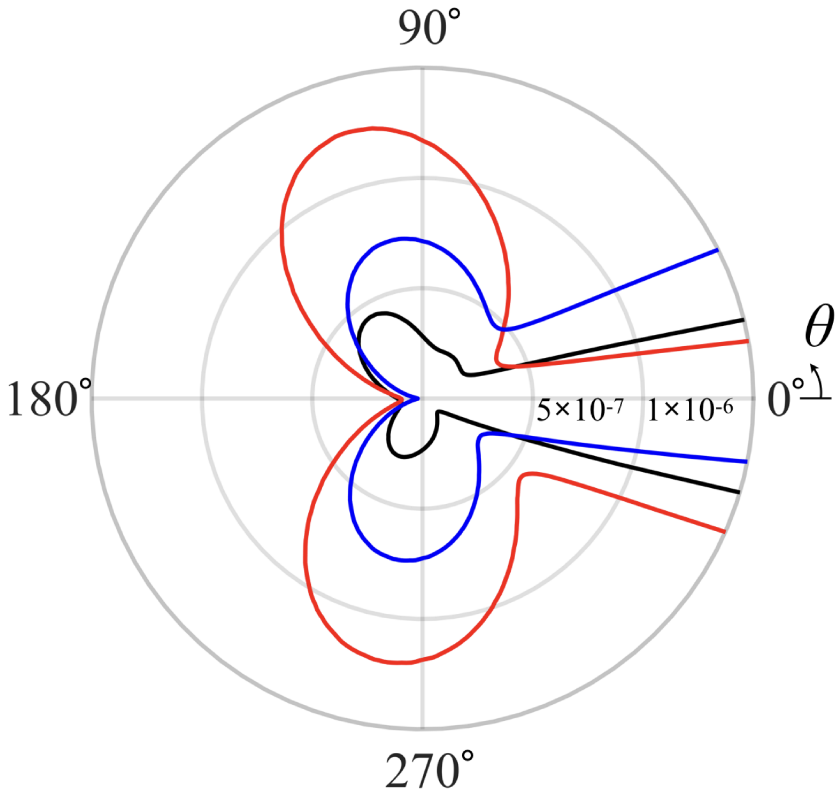

Fig. 11 Directivity of acoustic power at $\alpha = -4°$ (red line), $\alpha = 0°$ (black line), and $\alpha = 4°$ (blue line).

Spectra of p' at $r = 3.5$ in both cases are calculated via FFT with Hamming windows and no data overlapping (Figs. 12 and 13). At $\alpha = -4°$, the dominant acoustic generation comes from the frequency $f \sim 1.1$, which corresponds to the vortex shedding frequency of the wake at the airfoil trailing edge. It nearly covers all directions of the airfoil except vanishing near $\theta = 180°$. At $f = 1.8$ ($St_{W,1,-4°}$) and $f = 3.6$ ($St_{W,2,-4°}$), the p' spectrum also show local peaks indicating the acoustic generation of the flow dynamics near the cavity. The acoustic generation at $St_{W,1,-4°}$ mainly covers the second and the third quadrants whereas that at $St_{W,2,-4°}$ focuses on the second quadrant, but it has minor contribution in the first quadrant. The results suggest that the acoustic generation due to the cavity concentrates on the upstream of the cavity side, especially for the higher modes.

The acoustic generation at $\alpha = 4°$ is similar to that at $\alpha = -4°$. The vortex shedding at the airfoil trailing edge contributes the most to the acoustic generation as most of the peaks in Fig. 13 are at $f < 2$, which correspond to the peaks shown in Fig. 6b. These generations also covers all directions except $\theta = 180°$. Besides, the flow dynamics at the cavity also generate the acoustics at $f > 2$. They have upstream preference especially on the cavity side, leading to a minor contribution in the lower half of the airfoil.

According to Lam and Leung [1], the acoustic generation at $\alpha = 0°$ possesses contributions from different types of flow dynamics. In addition to vortex shedding at cavity and at airfoil trailing edge, a feedback mechanism between cavity and airfoil trailing edges also generates significant acoustics. These processes all occur in close frequencies and give rise to a great difficulty in discerning their contribution. However, such difficulty is not encountered with the present results with non-zero α. The flow dynamics at the cavity and the vortex shedding at the airfoil trailing edge operates at distinct frequencies in these two cases. Nevertheless, further analyses are still required to confirm the details of the mechanisms of the acoustic generation.

V. Conclusion

A numerical study of the aeroacoustics of NACA 0018 airfoil with a cavity at angles of attack $\alpha = -4°$ and $4°$ is reported. The Reynolds number based on airfoil chord length is fixed at 2×10^4. The presence of the cavity in essence

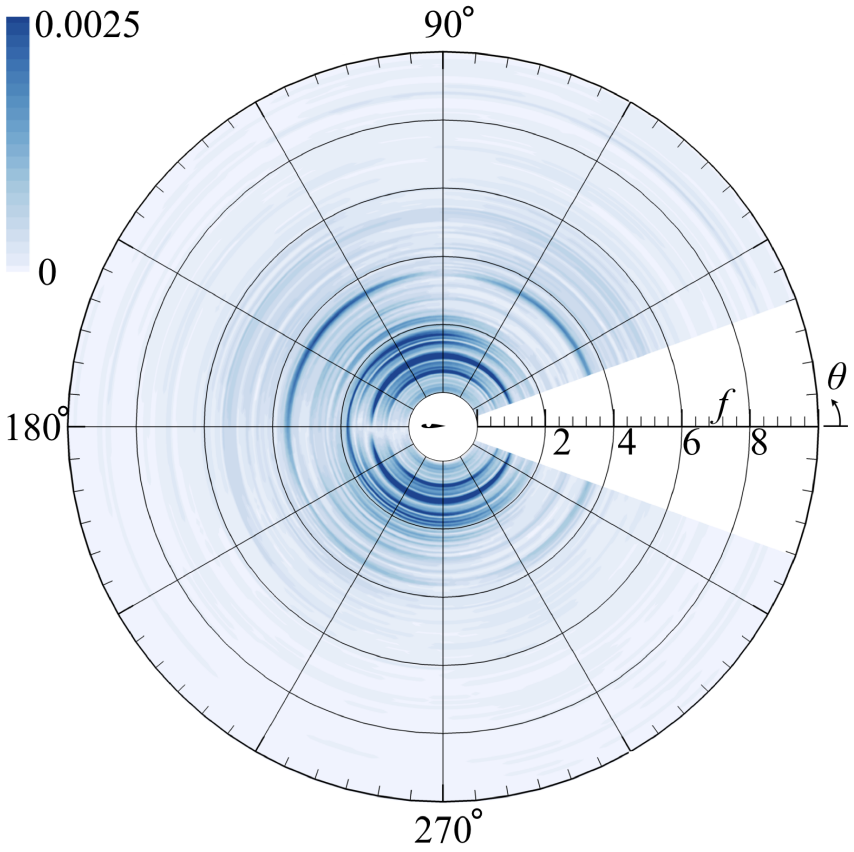

Fig. 12 Spectral directivity of p' at $r = 3.5$ ($\alpha = -4°$).

modifies the unsteady aerodynamics and the associated acoustic generation processes of the airfoil. At $\alpha = -4°$, the airfoil produces slightly higher lift than an ordinary airfoil does. This matches those reported in the literature. However, at $\alpha = 4°$, the airfoil generates less lift than those reported in previous research. The reason remains unclear and requires further investigations.

At both α, vortex shedding at the airfoil trailing edge is found to be the essential source of flow unsteadiness. The shear layer on the suction side at $\alpha = -4°$ separates early from the airfoil and sheds vortices before reaching the airfoil trailing edge. On the airfoil pressure side, the shear layer at the cavity oscillates vigorously with Mode I oscillation and shed vortices that are convected downstream and form vortex pairs with those shed on the suction side downstream of the airfoil trailing edge. At $\alpha = 4°$, the shear layer attaches to the airfoil until it reaches the airfoil trailing edge where vortices are shed to form the vortex street. In the vicinity of the cavity, the shear layer undergoes Mode II oscillation, which covers the whole cavity and oscillates mildly. A vortical structure is attached inside the cavity near the trailing edge which induces secondary vortices conveyed inside the cavity. Wavelet analyses of velocity fluctuations on the probes inside the cavity and in the wake of the airfoil reveal little switching between different types of flow dynamics. This observation is contradictory to the previous work with $\alpha = 0°$. Furthermore, different frequencies of these flow dynamics at both α suggest a weak interaction between them.

In regard to the acoustic generation, vortex shedding at the airfoil trailing edge dominates the generation especially at $\alpha = 4°$. The acoustic generation displays strong upstream preference for both α especially on the cavity side. The acoustic power generated is consistently higher than that in $\alpha = 0°$ case. Spectral analyses at $r = 3.5$ illustrate distinct contributions from different flow dynamics. This is completely different from the case with $\alpha = 0°$, in which all generating mechanisms produce acoustics at close frequencies leading to a great difficulty in discerning their individual contributions.

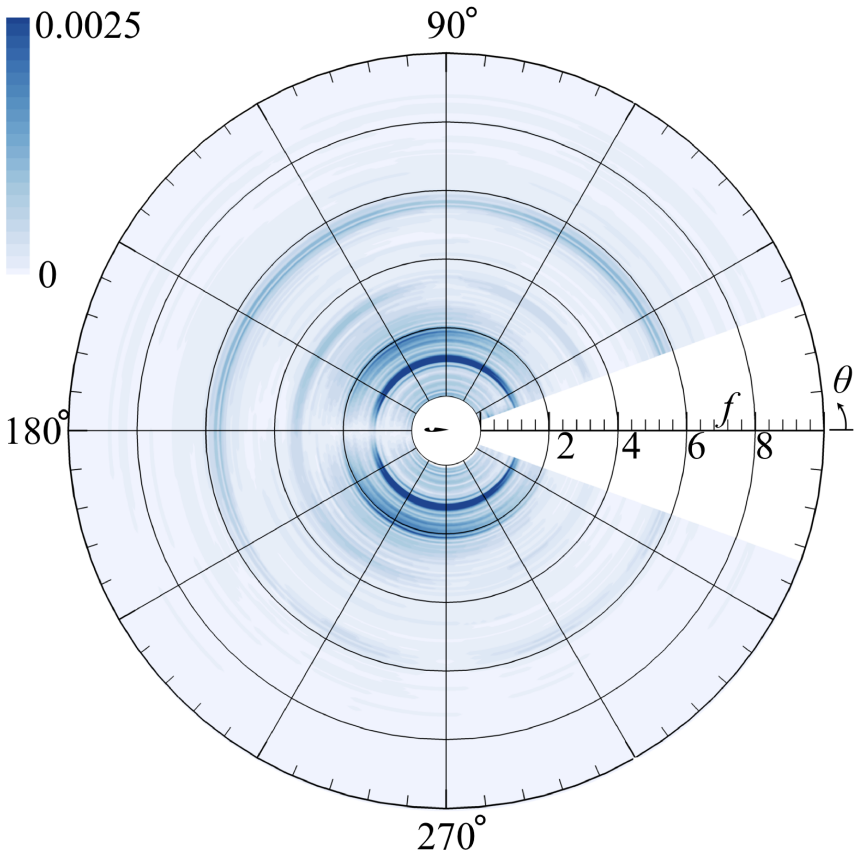

Fig. 13 Spectral directivity of p' at $r = 3.5$ ($\alpha = 4°$).

Acknowledgments

The authors gratefully acknowledge the support given by the Central Research Grant of The Hong Kong Polytechnic University under grant no. G-YBGF. The second author acknowledges the support given by a research donation from Philip K. H. Wong Foundation under grant no. 5-ZH1X and with a research project of the State Key Laboratory of Mechanical System and Vibration of Shanghai Jiao Tong University under grant no. MSV201404.

References

[1] Lam, G. C. Y., and Leung, R. C. K., "Aeroacoustics of NACA 0018 Airfoil with a Cavity," *AIAA Journal*, 2018, p. accepted.

[2] Kasper, W., "Aircraft wing with vortex generation," *US Patents US3831885 A*, 1974.

[3] Bunyakin, A. V., Chernyshenko, S. I., and Stepanov, G. Y., "Inviscid Batchelor-model flow past an airfoil with a vortex trapped in a cavity," *Journal of Fluid Mechanics*, Vol. 323, 1996, pp. 367–376.

[4] Bunyakin, A. V., Chernyshenko, S. I., and Stepanov, G. Y., "High-Reynolds-number Batchelor-model asymptotics of a flow past an aerofoil with a vortex trapped in a cavity," *Journal of Fluid Mechanics*, Vol. 358, 1998, pp. 283–297.

[5] Chernyshenko, S. I., Galletti, B., Iollo, A., and Zannetti, L., "Trapped vortices and a favourable pressure gradient," *Journal of Fluid Mechanics*, Vol. 482, 2003, pp. 235–255.

[6] Lasagna, D., Donelli, R., De Gregorio, F., and Iuso, G., "Effects of a trapped vortex cell on a thick wing airfoil," *Experiments in Fluids*, Vol. 51, No. 5, 2011, pp. 1369–1384.

[7] Olsman, J. W. F., and Colonius, T., "Numerical Simulation of Flow over an Airfoil with a Cavity," *AIAA Journal*, Vol. 49, No. 1, 2011, pp. 143–149.

[8] Olsman, W. F. J., Willems, J. F. H., Hirschberg, A., Colonius, T., and Trieling, R. R., "Flow around a NACA0018 airfoil with a cavity and its dynamical response to acoustic forcing," *Experiments in Fluids*, Vol. 51, No. 2, 2011, pp. 493–509.

[9] Tutty, O., Buffoni, M., Kerminbekov, R., Donelli, R., De Gregorio, F., and Rogers, E., "Control of Flow with Trapped Vortices: Theory and Experiments," *International Journal of Flow Control*, Vol. 5, No. 2, 2013, pp. 89–110.

[10] Lasagna, D., and Iuso, G., "Flow regimes in a trapped vortex cell," *Experiments in Fluids*, Vol. 57, No. 3, 2016, p. 36.

[11] Schumacher, K. L., Doolan, C. J., and Kelso, R. M., "The effect of a cavity on airfoil tones," *Journal of Sound and Vibration*, Vol. 333, No. 7, 2014, pp. 1913–1931.

[12] Lam, G. C. Y., Leung, R. C. K., Seid, K. H., and Tang, S. K., "Validation of CE/SE Scheme in low Mach number direct aeroacoustic simulation," *International Journal of Nonlinear Sciences and Numerical Simulation*, Vol. 15, No. 2, 2014, pp. 157–169.

[13] Lam, G. C. Y., Leung, R. C. K., and Tang, S. K., "Aeroacoustics of duct junction flows merging at different angles," *Journal of Sound and Vibration*, Vol. 333, No. 18, 2014, pp. 4187–4202.

[14] Loh, C. Y., and M. Q. Zaman, K. B., "Numerical investigation of transonic resonance with a convergent-divergent nozzle," *AIAA Journal*, Vol. 40, No. 12, 2002, pp. 2393–2401.

[15] Loh, C. Y., and Hultgren, L. S., "Jet Screech Noise Computation," *AIAA Journal*, Vol. 44, No. 5, 2006, pp. 992–998.

[16] Olsman, W. F. J., "Influence of a cavity on the dynamical behaviour of an airfoil," PhD, Technische Universiteit Eindhoven, 2010.

[17] Lam, G. C. Y., and Leung, R. C. K., "Sound generation by an in-flight thick airfoil with a cavity," *Proceedings of the 45th International Congress and Exposition on Noise Control Engineering*, edited by W. Kropp, Deutsche Gesellschaft fur Akustik e.V. (DEGA), Hamburg, 2016, pp. 6045–6055.

[18] Morfey, C. L., "Acoustic Power," *Dictionary of Acoustics*, Academic Press, London, 2001, p. 199.